공학석사 학위논문

A study on identifying noise sources in electric brake systems using dynamic characteristics analysis

전동식 브레이크 시스템의 동적 특성 분석을 이용한 소음원 규명에 대한 연구

2023 년 8 월

서울대학교 대학원

기계공학부

우 정 우

A study on identifying noise sources in electric brake systems using dynamic characteristics analysis

전동식 브레이크 시스템의 동적 특성 분석을 이용한 소음원 규명에 대한 연구

지도교수 강 연 준

이 논문을 공학석사 학위논문으로 제출함
2023 년 4 월

서울대학교 대학원
기계공학부
우 정 우

우정우의 공학석사 학위논문을 인준함
2023 년 6 월

위 원 장 도 형 록 (인)

부위원장 강 연 준 (인)

위 원 김 도 년 (인)

ABSTRACT

A study on identifying noise sources in electric brake systems using dynamic characteristics analysis

Jeongwoo Woo
School of Mechanical Engineering
The Graduate School
Seoul National University

This study investigates the operational mechanism of an electric brake system, analyzes the noise and vibration occurring during driving, and provides insights for enhancing NVH (Noise, Vibration, and Harshness) performance. Despite the inherent complexity of the brake system, accurately comprehending the dynamic characteristics of the entire system is indispensable. To address this, an assessment of noise frequencies generated during brake operation was conducted, coupled with capturing deformation shape information within the corresponding frequency bands. Comparative analyses of vibration levels and noise

were performed for each system component to unveil correlations. Additionally, employing a color map facilitated elucidating the relationship between rotational excitation and the system's response. Remarkably, when the rotational excitation component aligned with the system's natural frequency, an amplified response was observed. Consequently, dynamic modifications of key vibration components were implemented to circumvent resonance phenomena. Lastly, theoretical analysis of the motor and ball screw within the driving section, alongside experimental validation, elucidated the sources of noise and vibration as well as their performance characteristics.

Keywords: Electric brake system, Color map, Experimental modal analysis, Operational deflection shape, Order Analysis, NVH performance

Student Number: 2021-21541

TABLE OF CONTENTS

LIST OF TABLES

LIST OF FIGURES

CHAPTER 1

INTRODUCTION

As the global interest in green initiatives continues to rise, car manufacturers worldwide are responding by implementing major changes in response to new technological trends. One of the most prominent developments in this transformation is the ongoing development of electric vehicles (EVs), which use electric motors instead of traditional internal combustion engines. This change is providing consumers with new experiences and generating higher demand for EVs. While EVs offer a more peaceful environment due to the electrification of the powertrain that eliminates the noise and vibration characteristic of traditional engines, various NVH issues are arising as noise and vibration from other vehicle components that were previously masked by the engine become apparent. Despite these challenges, the use of electrification in subsystems such as braking and steering systems is gaining popularity because of the significant benefits of reduced weight and improved braking efficiency. Many of these vehicle subsystems use a common mechanism that employs a combination of a motor and a ball screw with rotating components. However, the vibration generated during the motor's rotation to produce braking pressure can excite the entire system and ultimately degrade the overall riding

experience. It is important to fundamentally address and mitigate the NVH issues that stem from these advances in order to improve the comfort and overall experience of vehicle occupants.

To analyze the sources of noise and vibration, numerous studies have been conducted. The paper by Zhu et al. [1-2] investigated how the cogging torque caused by slots affects the noise and vibration of permanent magnet synchronous motors. They found that the radial electromagnetic force density distribution from the slot magnetic field was the main cause of NVH deterioration in the motor, and they identified the harmonic components. Other studies by Gieras [3-4], Ren et al. [5], and Zhu and Howe [6] confirmed that cogging torque components were generated in motors and identified the sources of vibration and noise generated during motor rotation using order analysis. Lee et al. [7] determined the ball pass order of a ball screw by utilizing the ball pass frequency of a rotating rolling bearing. While many studies have used formulas and finite element method (FEM) analysis for rotating bodies, establishing the correlation between theoretical and experimental approaches is difficult in practical applications due to the use of complex systems comprising multiple components. This paper investigates the noise and vibration characteristics of electric brake systems and employs modal testing and operational deflection shape (ODS) analysis to select the analysis targets. It proposes suitable

experimental methods for NVH (Noise, Vibration, and Harshness) analysis and identifies the root causes of noise and vibration in electric brake systems through rigorous theoretical analysis and comprehensive experimental validation.

CHAPTER 2

THEORY

2.1 Rotational harmonic order

2.1.1 Motor

This study examines the use of an electric motor in a brake system, specifically a 10-pole 12-slot permanent magnet synchronous motor (PMSM). The PMSM has several advantages, including low driving losses, high efficiency, and a simple structure that makes it easy to maintain. The rotor of the PMSM has permanent magnets that create changes in the magnetic field of the air gap, which can cause cogging torque at high speeds. This torque results in uneven torque and motor noise. The rotor moves in the direction of the minimum magnetic resistance during motor operation, which causes the cogging torque. Furthermore, variations in the air gap in the motor can obstruct the flow of magnetic flux, leading to the formation of a radial electromagnetic force density distribution in the air gap magnetic field, which is described by Eq. (2.1).

$$F_r = B_g^2 / 2\mu_0 \tag{2.1}$$

Where F_r is the radial force density, B_g is the airgap flux density, and μ_0 is the permeability in a vacuum. In this case, the harmonic order component due to the rotor magnetic field of a synchronous motor is also a cause of noise and vibration, and the order r is given by Eq. (2.2).

$$r = (1 \pm 2k)p \tag{2.2}$$

Additionally, the order component caused by interaction between the rotor and the slots is given by Eq. (2-3).

$$r = |iN_s \pm np| \tag{2.3}$$

Where r, k are integers, n is odd, N_s and p are the number of slots and poles, respectively. If the pole and slot numbers of the motor are known using Eqs. (2.1) and (2.3), the order component generated by the motor can be calculated. The cogging torque frequency is determined by the least common multiple of the pole and slot numbers of the motor, as shown in Eq. (2-4), and the magnitude is determined by the radial and tangential flux densities.

$$f_c = k\frac{RPM}{60} \times LCM(N_s, p) \tag{2.4}$$

The LCM denotes the "Least Common Multiple" and k is an integer. Additionally, order components corresponding to multiples of the pole and slot numbers and their harmonics are sequentially generated.

2.1.2 Ball screw

Ball screws are a common mechanical component utilized in various machine systems to transform rotary motion into linear motion under axial load. During ball screw rotation, frequencies such as ball pass frequency of the shaft (BPFS), ball pass frequency of the nut (BPFN), and ball spin frequency (BSF) are produced, among which BPFS generates the most significant vibration with the largest amplitude. Lee, Won Gi[7] introduced an effective factor to calculate the BPFS for a rotating cloud bearing and applied it to ball screws. The BPFS of a ball screw can be evaluated using Eq. (2-5).

$$BPFS = \frac{n}{120}\frac{\sqrt{L_p^2 + (\pi D_b)^2}}{D_w}\left(1 + \frac{D_w}{\sqrt{L_p^2 + (\pi D_b)^2}} cos\,\alpha\right) \qquad (2.5)$$

α is the contact angle, n is the speed of the shaft, L_p is the lead of the screw, D_w is the ball diameter, and D_b is the screw diameter.

2.2 Plate analysis

2.2.1 Wave of plate

Among the various modes of vibration in a plate, the mode that exerts the strongest influence on vibration is the bending mode. Bending waves occur as vertical oscillations on the surface of the plate and are associated with the bending motion of the plate. These bending waves are determined by factors such as the shape, material, and boundary conditions of the plate, and they have a significant impact on the structural characteristics and vibration phenomena of the plate. On the other hand, longitudinal waves propagate along the surface of the plate, inducing horizontal vibrations, while transverse waves propagate perpendicular to the surface, causing vibrations parallel to the plate's surface. Although both longitudinal and transverse waves contribute to plate vibration, their influence is relatively smaller compared to bending waves.

2.2.2 Mode frequency of plate

The bending wave equation for a uniform flat plate can be derived through several assumptions. The plane wave propagates purely in the x-direction, and the plate is located in the x-z ($y = 0$) plane. Utilizing these assumptions, the wave equation for a thin plate can be obtained as follows[8].

$$D\left(\frac{\partial^4\eta}{\partial x^4}+2\frac{\partial^4\eta}{\partial x^2\partial z^2}+\frac{\partial^4\eta}{\partial z^4}\right)=-m\frac{\partial^2\eta}{\partial t^2} \tag{2.6}$$

$$D=\frac{Eh^3}{12(1-\nu^2)} \tag{2.7}$$

In this context, η represents the displacement, m denotes the mass per unit area of the plate, E is the Young's modulus, v represents the Poisson's ratio, and I represents the second moment of area per unit width. For a plate with thickness h, the value of $I = h^3/12$, allowing us to substitute D with the expression given in equation (2.7). By neglecting shear deformation and rotary inertia effects in the plate and assuming a simple harmonic motion for the displacement, the frequency of bending waves can be expressed as follows[8].

$$k_b^2=k_x^2+k_z^2 \tag{2.8}$$

$$k_b=\left(\frac{\omega^2 m}{D}\right)^{1/4} \tag{2.9}$$

For a finite plate with dimensions of length a in the x-direction and b in the z-direction, equation (2.8) can be expressed as equation (2.10), allowing us to calculate the bending wave frequencies in the (p, q) modes of the plate.

$$k_b^2=k_x^2+k_z^2=\left(\frac{p\pi}{a}\right)^2+\left(\frac{q\pi}{b}\right)^2=\left(\frac{\omega^2 m}{D}\right)^{1/2} \tag{2.10}$$

In this case, p and q are integers, and the resonance frequencies in the (p, q) mode can be calculated using Equation (2.10). By doing so, it is possible to predict the mode frequencies of a thin plate, which can be utilized in the design of noise and vibration reduction strategies for structures[8].

$$f_{pq} = \frac{1}{2\pi}\left(\frac{D}{m}\right)^{1/2}\left[\left(\frac{p\pi}{a}\right)^2 + \left(\frac{q\pi}{b}\right)^2\right] \tag{2.11}$$

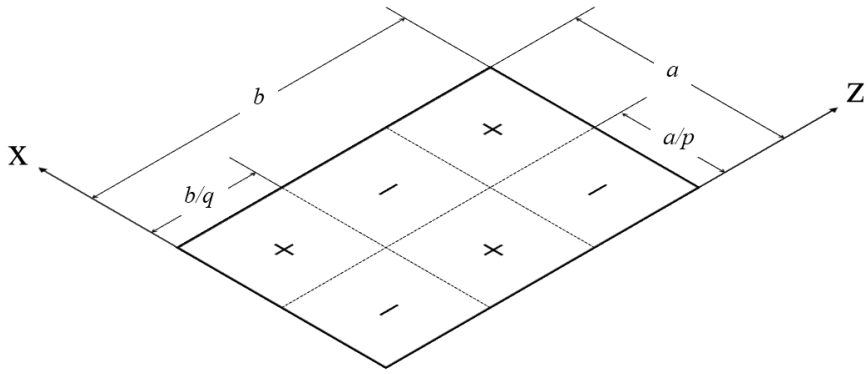

Figure 2.1 Nodal lines and phases of a vibrating rectangular panel

CHAPTER 3

EXPERIMENTAL PROCEDURES

3.1 Experimental design for NVH characteristic analysis

3.1.1 Experimental setup

Braking plays a critical role in ensuring vehicle safety and performance. To optimize vehicle design and improve NVH performance, it is crucial to have a thorough understanding of the braking system's response characteristics. In this study, we aimed to capture the dynamic response characteristics of the braking system by installing acceleration sensors in each component. Figure 3.1, 3.2 and Table 3.1 provide an overview of the installed sensors, enabling us to analyze the behavior of individual components under various braking scenarios.

Furthermore, we simulated harsh braking conditions, such as sudden stops during normal vehicle operation. To accurately evaluate the dynamic response of the braking system under these conditions, we implemented a pressure control method. This approach allowed us to measure objective performance without directly manipulating the brake pedal, providing valuable insights into

the dynamic behavior of the system and facilitating a comprehensive assessment of its performance metrics.

Simultaneously, we conducted measurements of vibrations and noise generated during braking. By employing advanced measurement techniques, we ensured the reproducibility of our experimental setup, conducting tests multiple times under identical conditions. This comprehensive analysis of the braking system's vibration and noise characteristics deepened our understanding of its operational behavior.

3.1.2 Experimental measurement

The measurement results of the operating noise in the electric brake system revealed a prominent noise peak occurring within the range of 3000 Hz. Subsequently, a meticulous vibration response analysis was conducted specifically at this frequency to gain deeper insights into the system's behavior. Instead of relying on specific accelerometer measurements, a data averaging approach was adopted to capture the vibration characteristics of individual components.

Significantly, a strong correlation between the noise and vibration data was observed, confirming the coherence between these two factors, as depicted in

Figure 3.3. Accordingly, the targeted frequency range associated with the noise peak was determined, and components exhibiting elevated vibration levels within this range were identified for further investigation.

Among the various components, the motor and electronic control unit (ECU) cover exhibited notably higher vibration responses compared to others. To validate the observed vibration responses, operational deflection shape (ODS) data were employed to assess the deformation patterns of the selected components. Figure 3.4 clearly illustrates substantial deformation in these components, corroborating the presence of vibration-related issues. Notably, the ECU cover demonstrated the highest vibration level at 960 Hz, emphasizing the need for an in-depth analysis of the noise and vibration sources within this frequency band.

By integrating the noise and vibration analysis, our study not only pinpointed the specific frequency range associated with the noise peak in the electric brake system but also established a robust correlation between noise and vibration characteristics. Furthermore, the identification of components with heightened vibration levels offers valuable insights for further analysis and targeted improvements in the design and performance of the brake system.

3.2 Verification of results

3.2.1 Modal Analysis

To conduct a detailed analysis of the phenomena occurring at the frequencies associated with the maximum noise and vibration levels, an experimental modal analysis was performed on the ECU cover, which exhibited the highest response. Modal analysis, a fundamental method for determining the mode frequencies of a system, was employed in this study. It was hypothesized that the response would be significantly amplified due to the resonance of the components during system operation. Initially, four accelerometers were utilized during the initial drive test on the ECU cover, but to ensure precise analysis of the mode shapes, the number of sensors was increased to eleven. The positions of these sensors and the geometry of the ECU cover are presented in Figure 3.5.

The results of the modal analysis revealed the presence of various mode shapes distributed within the high-frequency range where the vibration level of the ECU cover was prominent. Notably, modes such as bumping, torsion, bending, and mixed modes were observed, as illustrated in Figure 3.6.

The modal frequencies of the ECU cover obtained from experimental modal analysis were also theoretically validated. The ECU cover was modeled

as a thin plate, assuming a rectangular shape, and the equations introduced in the previous section were utilized to calculate the (p, q) mode frequencies. By referring to Table 3.2, it was observed that the frequency ranges of the (1,1), (1,2), (2,1), and (1,3) modes corresponded accurately. However, it should be noted that this frequency difference was obtained by assuming a flat plate without considering the depth variations occurring in the actual cover. Thus, the consistency of the mode frequency ranges was confirmed using a simplified model.

3.2.2 Comparing SPL by modifying dynamic characteristics

The influence of the resonant behavior of the ECU cover and the potential for resonance avoidance were investigated by intentionally modifying the dynamic characteristics of the component within the mode frequency distribution range. The mode shape at 680 Hz, as observed in Figure 3.6, exhibited significant motion at the center of the cover, indicating a bumping mode. To understand the trend in noise levels through local characteristic modifications, mass was attached to the center of the cover, resulting in a reduction of approximately 15 dB in the noise level at 680 Hz, as shown in Figure 3.7.

To assess the effects of bending, torsion, and mixed modes, damping material was applied to the front surface of the cover, as depicted in Figure 3.8, allowing for overall characteristic modifications. Attaching damping material led to an overall reduction in the noise level, particularly at frequencies of 1300 Hz and 1600 Hz, effectively mitigating the impact of bending and mixed modes on the ECU cover. However, suppressing the 980 Hz torsion mode, characterized by maximum displacement at the edges, proved challenging through frontal attachment alone. Therefore, to address this issue, the entire perimeter of the cover was covered, as depicted in Figure 3.9, resulting in a significant decrease in the noise level at the torsion mode frequency. The observed decrease in noise level resulting from the modification of the dynamic characteristics of the ECU cover verified that the noise within the target frequency range originated from the cover itself. These experimental findings provide valuable insights into the dynamic characteristics of the ECU cover and effectively demonstrate the trends in noise level through the manipulation of its properties.

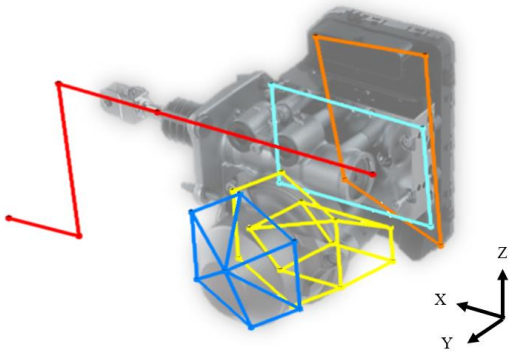

Figure 3.1 Geometry of the electric brake system

Table 3.1 Information of the components

Component	Classification (# of sensors)
Motor Assy	(7)
Cylinder Body	(12)
ECU Cover	(4)
HU Block	(4)
Pedal Assy	(5)

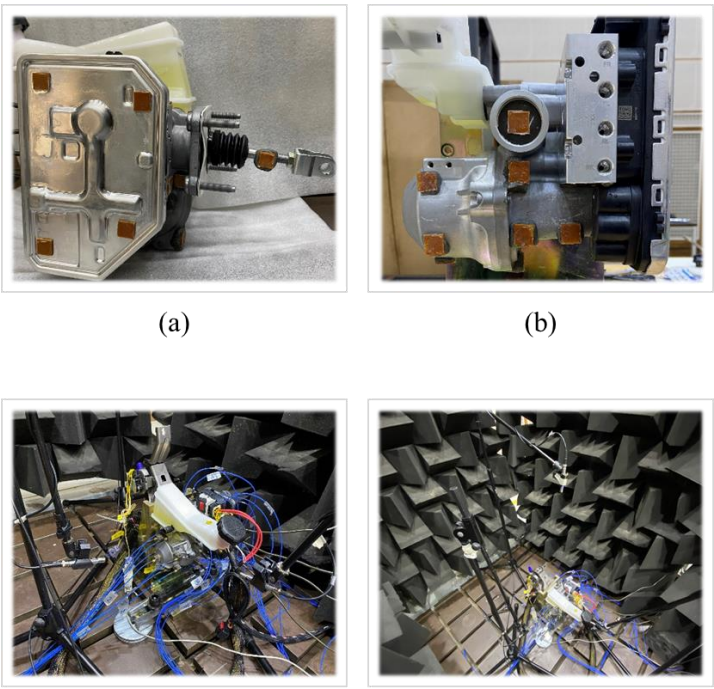

Figure 3.2 Accelerometer attachment locations and experimental setup of the brake system: (a) ECU Cover, (b) Motor assembly, Cylinder Body, HU Block, and (c) experimental setup, and (d) microphone placement

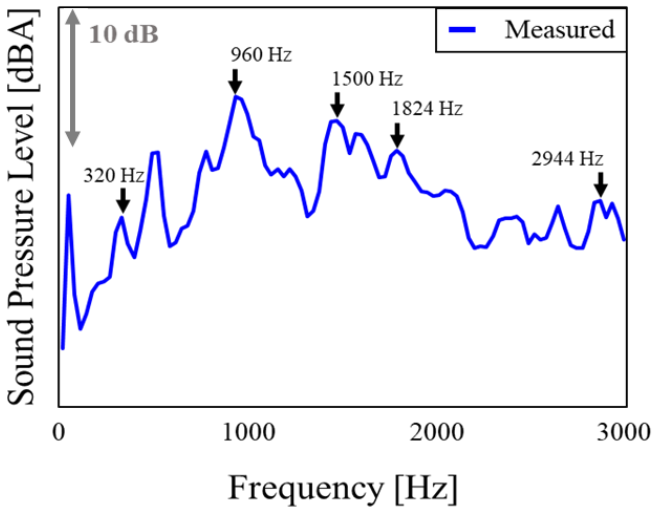

(a)

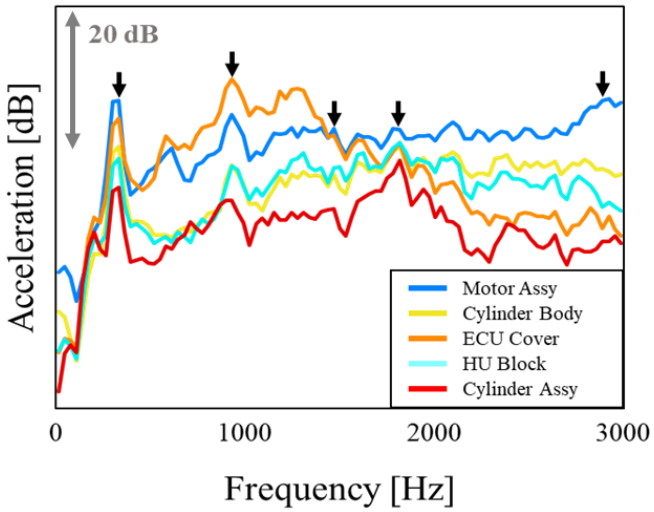

(b)

Figure 3.3 Measurement results of noise and vibration levels during electric brake operation: (a) microphone, and (b) accelerometer

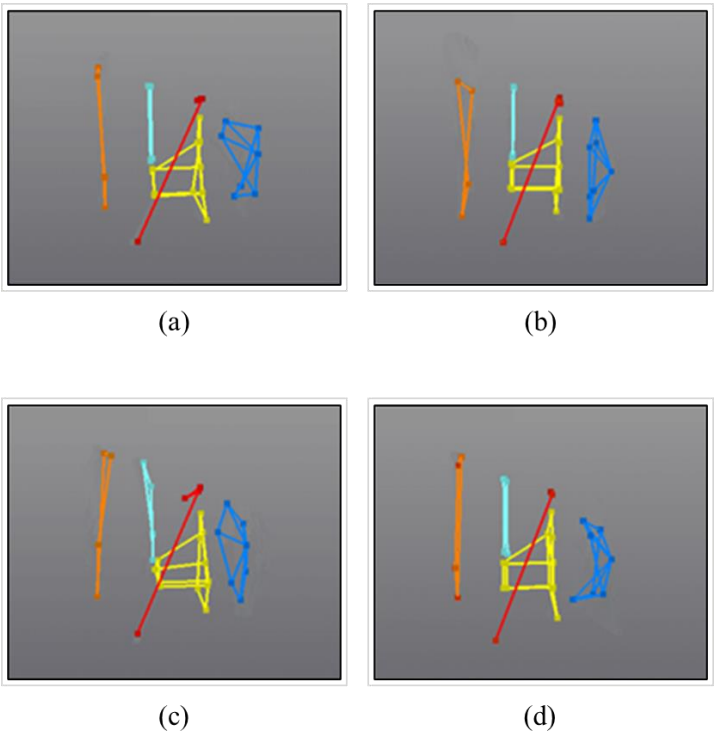

Figure 3.4 Operational deflection shapes at the target frequency: (a) 320 Hz, (b) 960 Hz, (c) 1824 Hz and (d) 2944 Hz

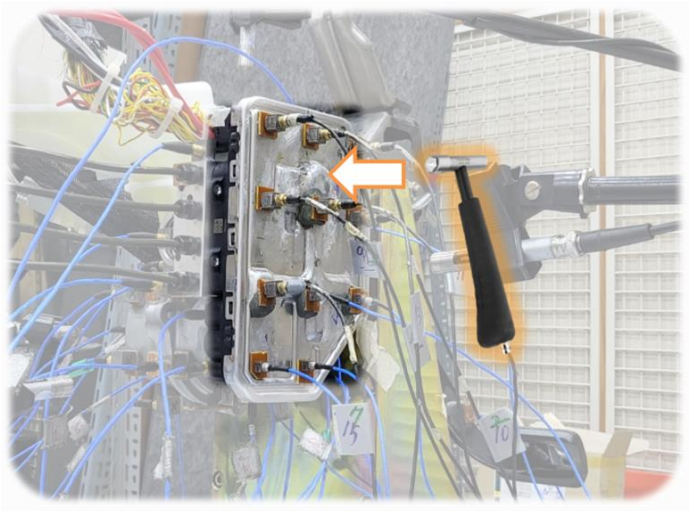

(a)

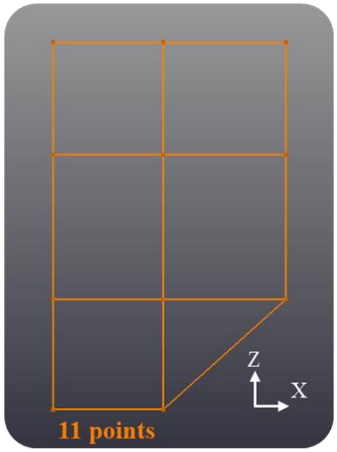

(b)

Figure 3.5 Experimental modal analysis setup: (a) location of accelerometer and excitation point, and (b) geometry of ECU Cover

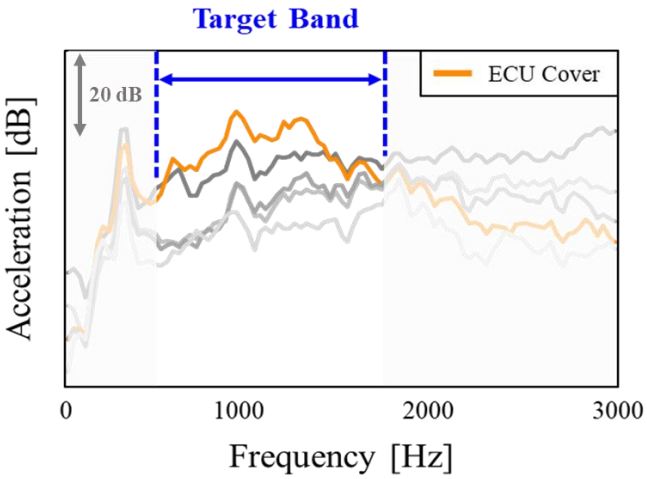

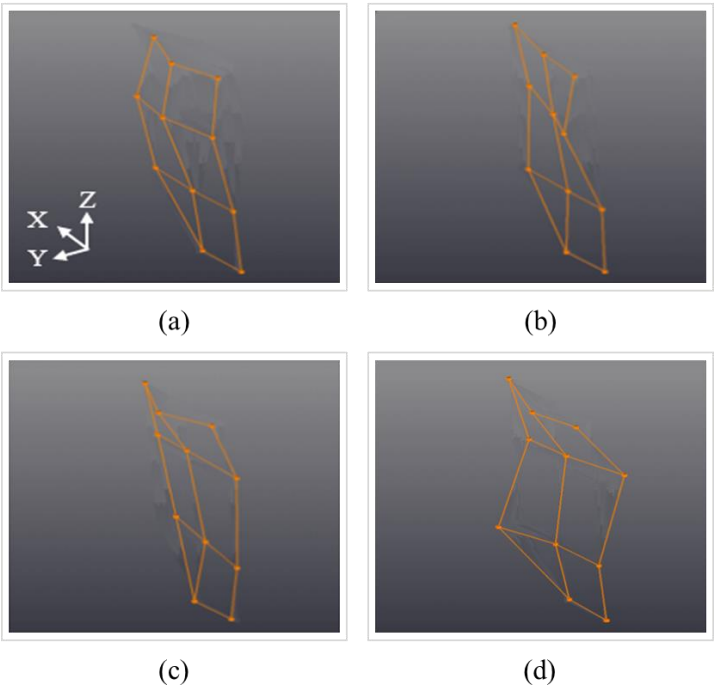

Figure 3.6 Target frequency range of the main vibration and mode shapes of the ECU Cover: (a) 680 Hz-bumping, (b) 980 Hz-torsion, (c) 1300 Hz-bending and (d) 1600 Hz-mixed

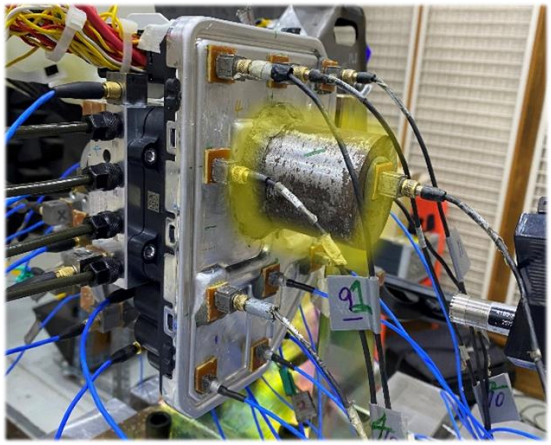

(a)

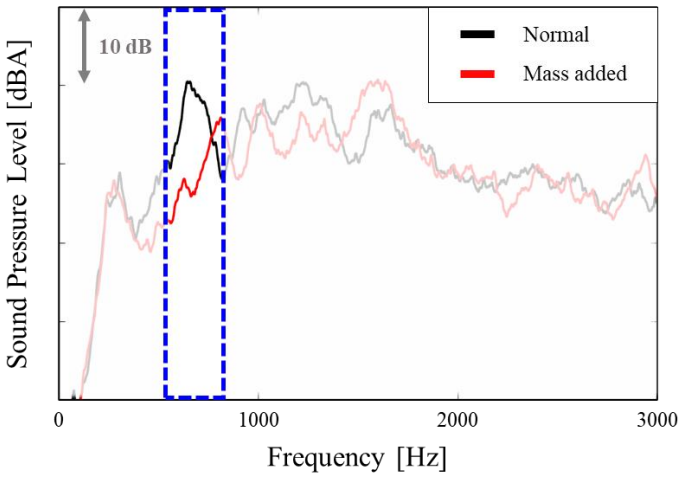

(b)

Figure 3.7 Modification of local dynamic characteristics through mass attachment to the ECU Cover: (a) experimental setup, and (b) comparison of sound pressure level(SPL) results

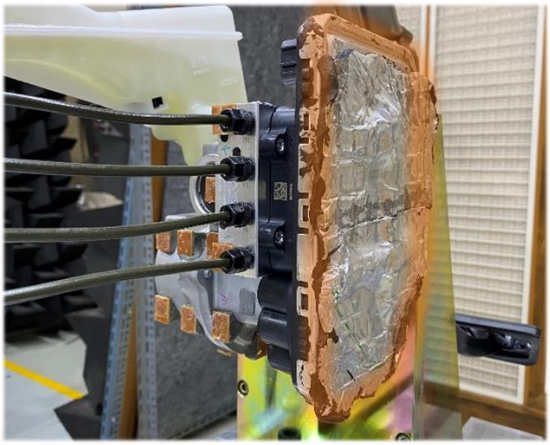

(a)

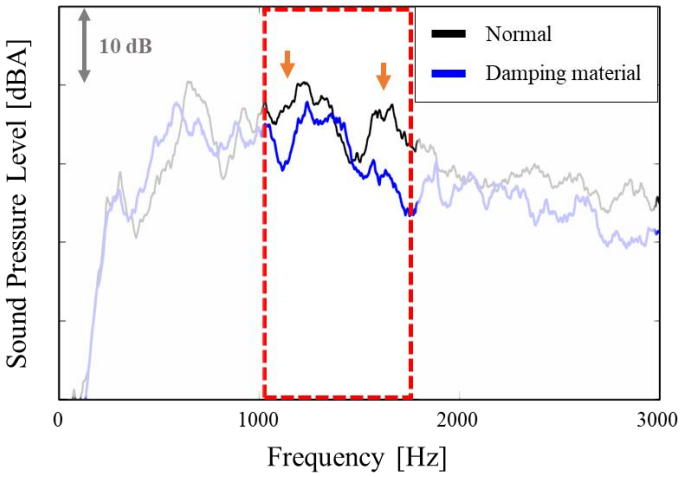

(b)

Figure 3.8 Modification of overall dynamic characteristics through frontal attachment of damping material to the ECU Cover: (a) experimental setup, and (b) comparison of sound pressure level(SPL) results

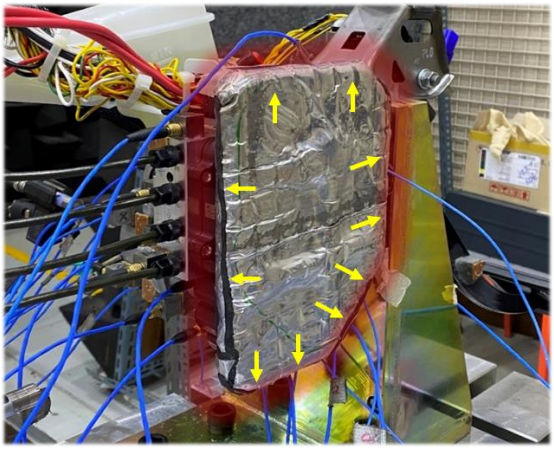

(a)

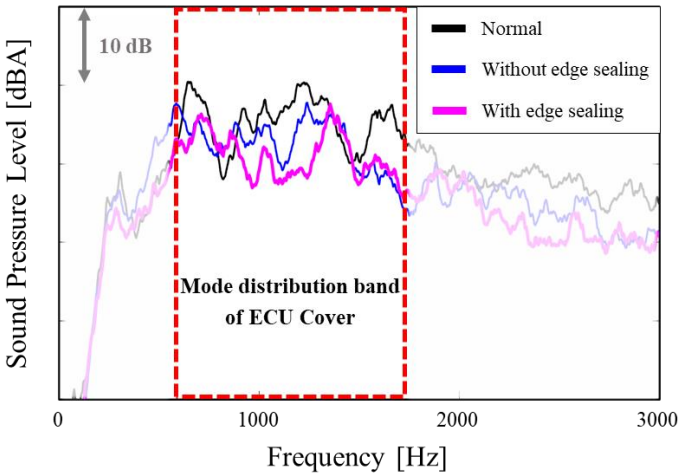

(b)

Figure 3.9 Modification of overall dynamic characteristics of the ECU Cover through frontal attachment of damping material, including the edges: (a) experimental setup, and (b) comparison of sound pressure level(SPL) results

Table 3.2 Theoretical (p, q) mode frequency results of the ECU Cover

(*p*, *q*) mode		***p***			
		1	2	3	⋯
q	1	425 Hz	833 Hz	1512 Hz	⋯
	2	1296 Hz	1703 Hz	2382 Hz	⋯
	3	2746 Hz	3153 Hz	3832 Hz	⋯
	⋮	⋮	⋮	⋮	⋱

CHAPTER 4

ORDER ANALYSIS

4.1 Rotational analysis of electric brake system

4.1.1 Mechanisms of vibration and noise generation

In Section 3.2, it was observed that the ECU cover plays a significant role in generating major noise and vibration levels. It was found that the mode frequencies of the ECU cover are excited by the driving force generated during brake operation. Furthermore, compared to other components, the motor assembly, which is a driving component, exhibited higher vibration levels across various frequency ranges. Therefore, a detailed analysis of the motor, as a crucial component of the electric brake system, is necessary.

Figure 4.1 illustrates the various mechanisms contributing to the generation of vibration and noise during brake operation. Firstly, the application of brake pressure activates the motor, leading to the generation of vibration. In electric brake systems, the motor receives power and rotates to produce the necessary braking force. This rotational motion of the motor, along with the conversion of electrical signals, results in the emission of noise and vibration, which are subsequently transmitted through the surrounding components and

structures. Secondly, the rotational excitation caused by rotating components significantly influences the vibration and noise levels of the brake system. Imbalances or distortions in these rotating parts can introduce vibration and noise into the system. Lastly, the overall response of the system plays a vital role in brake vibration and noise. The components within the system respond to external stimuli, and the interaction between these components can amplify the vibration and noise levels experienced. To analyze the phenomenon of noise generation during brake operation, a comprehensive approach such as order analysis is employed to examine the individual components contributing to vibration and noise.

4.1.2 Results of order analysis

In this study, order analysis was performed to analyze the rotational motion of the electric brake system, which is driven by the rotation of the motor and ball screw. Order analysis is commonly used to quantify the rotational frequency components of vibration and noise generated by the rotating components in a system. It helps to identify the rotational frequency components generated by the driving mechanism and track the main vibration sources of each component. Figure 4.2 presents the results of order analysis for

noise and vibration, and Table 4.1 provides the priority of order components for each component.

It was observed that the frequency range of the maximum response noise, corresponding to the driving RPM range of the motor, is associated with the 30th order component. This result indicates that high response noise can occur in specific frequency ranges due to motor operation. From the order analysis results for each component, it was determined that the three highest vibration levels were observed at the 10th, 53rd, and 70th order components. These components were observed across multiple components and are consistent with the noise order analysis results shown in Figure 4.2(a).

Based on these order analysis results, the range of the main order components was identified and presented in Figure 4.3. Particularly, a significant response was observed from the ECU cover in the 30th and 40th order frequency ranges of the motor. This indicates that high response noise can occur in specific frequency ranges due to motor operation, as mentioned earlier. Therefore, it can be inferred that the noise and vibration response tendencies of the system may vary depending on the order components of the motor's rotation. Additionally, it was observed that the 53rd order component, which is not a harmonic order component of the motor, was among the significant noise order

components. This component is likely to be caused by other factors within the system or external influences.

4.2 Verification of results

4.2.1 Theoretical approach

The system under investigation comprises a rotating mechanism consisting of a motor and a ball screw, as previously mentioned. The motor utilized in this study is a 10-pole 12-slot permanent magnet synchronous motor. Unlike conventional electric motors driven by electrical circuits, the permanent magnet synchronous motor generates rotational motion by harnessing the magnetic field produced by permanent magnets affixed to the rotor. However, the operation of this motor gives rise to noise and vibration issues attributable to the combined effects of mechanical and electromagnetic factors. These factors encompass cogging torque, electromagnetic forces arising from radial magnetic flux density, as well as suboptimal coupling between rotating components and mechanical parts [1-6]. Consequently, the fundamental frequency component of motor vibration, referred to as the Fundamental frequency, is found to correspond to the 10th harmonic, with sequential

occurrence of harmonic frequency components (30, 40, 70, 80). The validity of these observations can be theoretically substantiated using Eqs. (2.1)-(2.4).

As for the ball screw, an analysis was conducted by calculating the ball pass frequency for the rotating nut bearing, employing the effective factor. The results revealed a congruence between the ball pass frequency of the ball screw and the harmonics of its fundamental order [7]. Based on this analysis, it can be theoretically deduced that the 10th and 70th components of the motor, along with the 53rd component of the ball screw, manifest as the primary sources of system vibration, arising from the combined influence of electromagnetic and mechanical factors.

4.2.2 Experimental approach

In order to experimentally validate the rotational components of the motor derived theoretically, a systematic experimental procedure was conducted. Firstly, drive experiments were performed on the individual motor under unloaded conditions to measure the associated noise. As depicted in Figure 4.4, the presence of components corresponding to the 10th, 60th, and 70th orders was observed. These experimental findings are consistent with the theoretical

analysis of motor noise and vibration performed earlier, thus providing empirical confirmation of the motor's influence.

To investigate the impact of the ball screw, a specialized sample was fabricated by removing the ball screw within the electric brake system. Experimental order analysis was then conducted on this sample. The color map presented in Figure 4.5 reveals that, in comparison to the previous dataset, the identical motor exhibited the previously identified fundamental (10th order) and harmonic components. However, the 53rd-order component was not detected in the sample without the ball screw. This experimental analysis serves to demonstrate that the ball screw is the underlying source of the 53rd-order component and provides empirical evidence to support its influence, thereby aligning with the theoretically derived order components. Consequently, the verification of the ball screw's influence has been effectively accomplished.

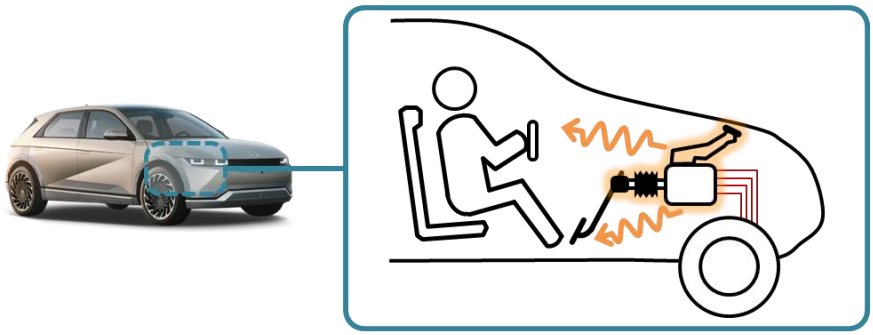

(a)

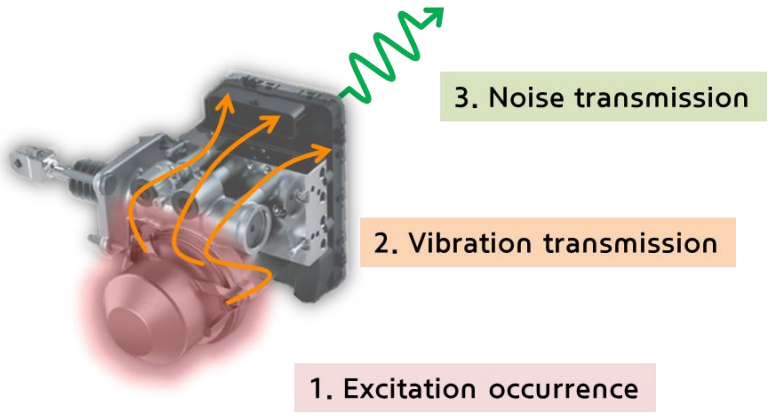

(b)

Figure 4.1 Mechanism of noise and vibration generation in electric brakes: (a) path of noise and vibration transmission and (b) source-path-receiver

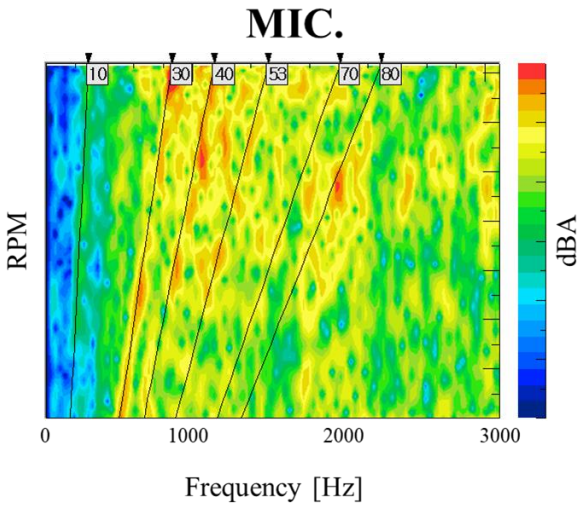

(a)

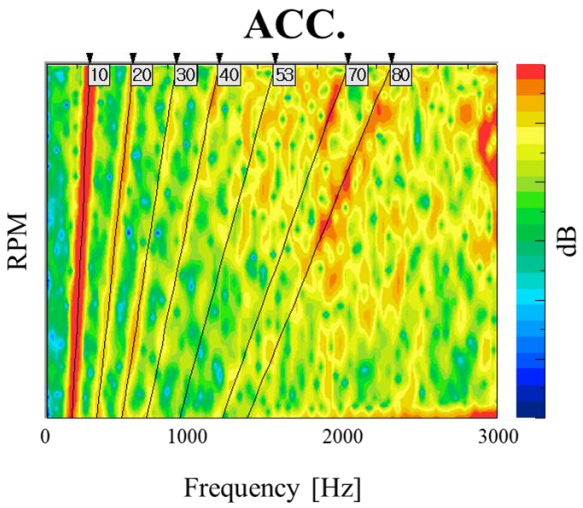

(b)

Figure 4.2 Order analysis results of noise and vibration during electric brake operation: (a) microphone, and (b) accelerometer

Table 4.1 Rotational excitation order for system components

Ranking	Components				
	Motor Assy	Cylinder Body	ECU Cover	HU Block	Pedal Assy
1st	10th	10th	30th	10th	58th
2nd	53rd	70th	10th	70th	70th
3rd	70th	60th	37th	53rd	10th

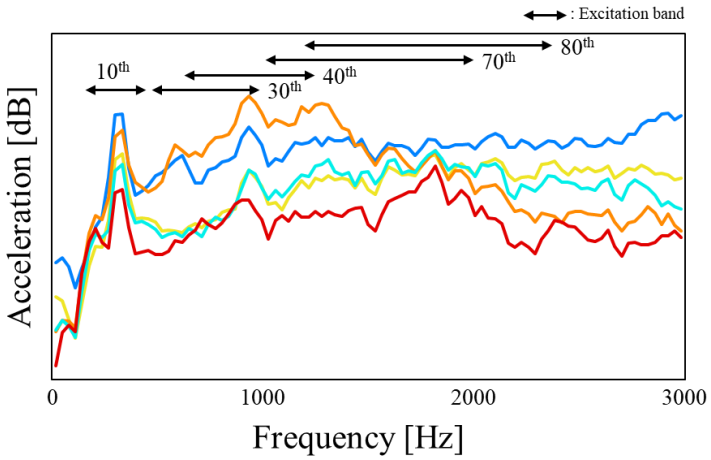

Figure 4.3 Excitation band of rotating excitation components at peak frequency during electric brake operation

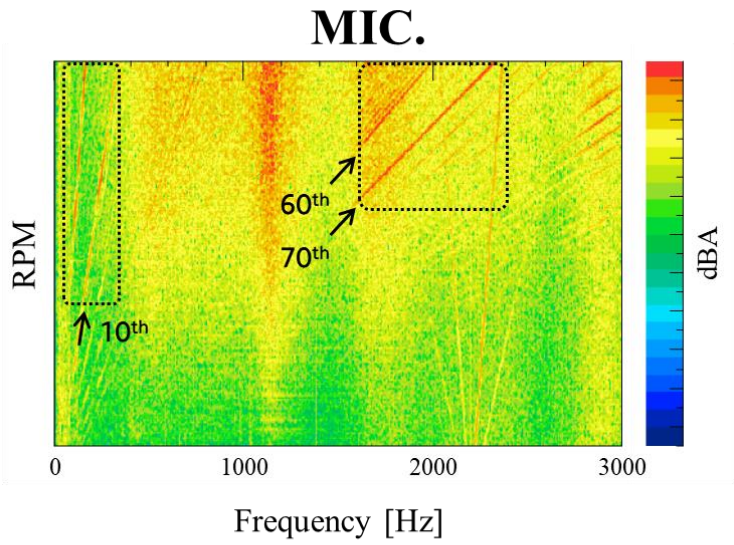

(a)

(b)

Figure 4.4 Experiment of un-loaded motor operation: (a) order analysis results of microphone, and (b) experimental setup

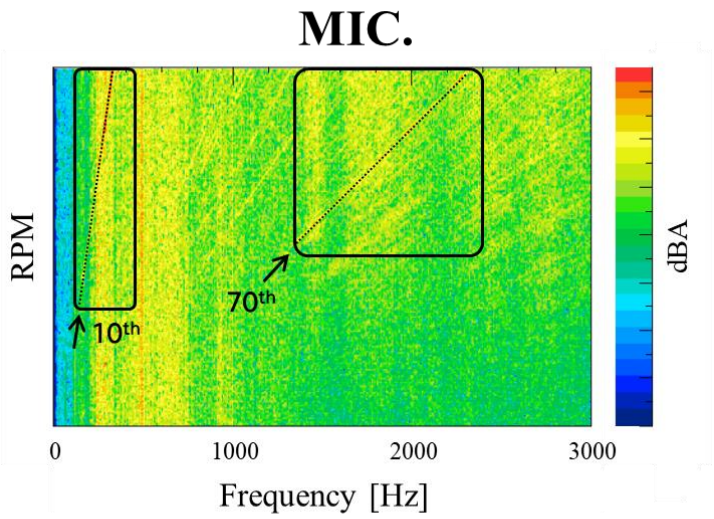

(a)

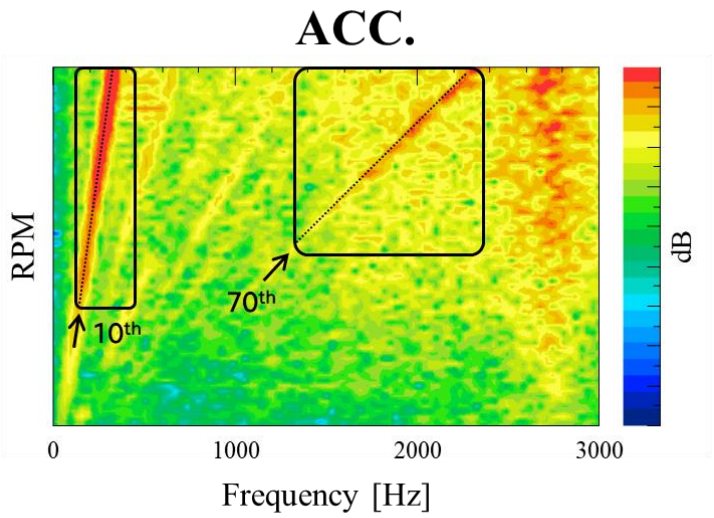

(b)

Figure 4.5 Order analysis results of noise and vibration during electric brake operation without a ball screw: (a) microphone, and (b) accelerometer

CHAPTER 5

CONCLUSION

In this study, the mechanism of vibration and noise generated during the braking process in an electric brake system was investigated to understand the phenomena and identify the underlying causes. The electric brake system experiences vibrations due to the interaction between the motor and other components, which are transmitted to the driver through the pedal, affecting driving comfort in addition to the operational noise. Therefore, it is crucial to accurately comprehend the dynamic characteristics of the brake system. Accordingly, this research aims to present an analytical process for practical issue resolution.

During the research process, the dominant noise frequencies generated during brake operation were identified, and the vibration levels of each component within those frequency ranges were determined using deformation information obtained during operation. Furthermore, order analysis was conducted using color map information to identify the significant rotating excitation components of the system. Experimental modal analysis was performed to gain insights into the dynamic characteristics of the system and validate the correlation between static and dynamic analysis results. Through

these investigations, the primary causes of noise and vibration during the operation of the automotive brake system were clearly identified. The obtained research findings can contribute to practical issue resolution and contribute to the enhancement of NVH through the design improvement of electric brake systems.

REFERENCES

[1] Z. Q. Zhu, D. Howe, E. Bolte, and B. Ackermann, "Instantaneous magnetic field distribution in brushless permanent magnet DC motors. I. Open-circuit field," IEEE Trans. Magn., 29, 124-135 (1993).

[2] Z. Q. Zhu, Z. P. Xia, L. J. Wu and G. W. Jewell, "Analytical modeling and finite-element computation of radial vibration force in fractional-slot permanent-magnet brushless machines," IEEE Trans. Ind. Appl., 46, 1908-1918 (2010).

[3] J. F. Gieras, *Electrical machines: fundamentals of electromechanical energy conversion*, (CRC Press, Florida, 2016).

[4] J. F. Gieras, C. Wang and J. C. Lai, *Noise of polyphase electric motors*, (CRC Press, New York, 2006).

[5] W. Ren, Q. Xu, Q. Li and L. Zhou, "Reduction of cogging torque and torque ripple in interior PM machines with asymmetrical V-type rotor design," IEEE Trans. Magn., 52, 1-5 (2016).

[6] Z. Q. Zhu and D. Howe, "Influence of design parameters on cogging torque in permanent magnet machines," IEEE Trans. Energy Convers., 15, 407-412 (2000).

[7] W. G. Lee, J. W. Lee, M. S. Hong, S. H. Nam, Y. H. Jeon and M. G. Lee, "Failure diagnosis system for a ball-screw by using vibration signals", Shock Vib., 2015 (2015).

[8] F. J. Fahy, *Sound and structural vibration: radiation, transmission and response*, 2nd ed. (Elsevier, Oxford, 2007).

국 문 초 록

본 연구는 전동식 브레이크 시스템의 구동 메커니즘을 분석하여, 운전 중 발생하는 소음과 진동을 분석하고, NVH 성능을 향상시키기 위한 통찰력을 제공하기 위해 수행되었다. 브레이크 시스템의 복잡성으로 인해, 전체 시스템의 동적 특성을 정확하게 파악하는 것은 어려울 수 있으나, 이는 필수적인 과정이다. 이를 위해, 브레이크 작동 중 발생하는 소음 주파수를 평가하고 해당 주파수 대역에서 운전 중 변형 형상 정보를 얻었다. 이어서, 각 구성 요소의 진동 수준과 소음을 비교하여 상관 관계를 분석하였다. 또한 컬러맵을 활용하여 회전 가진의 영향과 시스템의 응답 사이의 관계를 확인하였다. 회전 가진 성분이 시스템의 고유 주파수를 가진할 경우, 더 높은 응답이 발생한다는 것을 확인하였다. 이에 따라, 주요 진동 구성 요소의 동적 특성을 변경함으로써 시스템 공진을 회피하고자 하였다. 마지막으로, 주요 구동부인 모터와 볼 스크류의 발생 소음 및 진동 발생 원인과 성능을 이론적으로 분석하고, 이를 실험 결과를 통해 검증하였다.

주요어 : 전기 브레이크 시스템, 컬러맵, 실험적 모달 분석,
운전 중 변형 형상, 차수 분석, NVH 성능
학 번 : 2021-21541